Preprints (www.preprints.org) | NOT PEER-REVIEWED | Posted: 20 September 2019 doi:10.20944/preprints201909.0237.v1

Article

Railway ballast monitoring by GPR: a test site investigation

Luca Bianchini Ciampoli*, Alessandro Calvi and Fabrizio D'Amico

[1] Department of Engineering, Roma Tre University, Via Vito Volterra 62, 00146, Rome, Italy
* Correspondence: luca.bianchiniciampoli@uniroma3.it; Tel.: +39 06 5733 3617

Abstract: Effective maintenance of railways requires a comprehensive assessment of the actual condition of the construction materials involved. In this regard, Ground-Penetrating Radar (GPR) stands as a viable alternative to the invasive and time-consuming traditional techniques for the inspection of these infrastructures. This work reports the experimental activities carried out on a test-site area within a railway depot in Rome, Italy. Specifically, a 30 m-long railway section was divided into 10 sub-sections reproducing different various physical and structural conditions of the track-bed. In more detail, combinations of varying scenarios of fragmentation and fouling of the ballast were reproduced. The set-up was then investigated using different multi-frequency GPR horn antenna systems. The effects of the different physical conditions of ballast on the electromagnetic response of the material were analysed for each scenario using time- and frequency-domain signal processing techniques. Parallel to this, modelling was provided to estimate fouling content. Interpretation of results has proven the viability of the GPR method in detecting signs of decay at the network level, thereby proving this technique to be worthy for implementation in asset management systems.

Keywords: gpr; ndt; railway; ballast fouling; ballast fragmentation; railway maintenance; transport infrastructure monitoring

1. Introduction

Railway convoys daily carry commuters, freights and bulk goods by traveling along ballasted tracks. The important role of railway transport in connecting residential and production poles has determined an improvement of the technical performance of the convoys that, in turn, require adequate support from the track-beds. To this effect, an ever effective and timely maintenance is needed for railway ballast in order to ensure suitable safety and functionality conditions over the network.

By literature, a typical railway track-bed can be schematized as the superposition of two construction systems, namely, the superstructure and the substructures [1, 2]. The superstructure composes of rails, fastening system and sleepers, whereas the substructure includes the granular layers that are laid upon the subgrade, i.e. the ballast and the sub-ballast. Specifically, ballast is referred to as a homogeneously graded hard-rock-derived material, usually composed of aggregates with a diameter size ranging between 3 and 6 cm [2, 3].

The bearing capacity of the substructure stands as a major concern for designers and maintainers, as differential settlements are usually reported to occur within this system [1, 4]. This is mainly due to *i)* the change in the material grading caused by the breakage of the sharp corners of the ballast aggregates under cycling loadings [5, 6] and *ii)* the pollution of the air voids by fine-graded material derived from the ballast-sleeper and the wheel-rail friction [4]. This can be directly poured by the passing freights [7] or it can migrate upwards or side wards from the subgrade along with capillary water [8].

© 2019 by the author(s). Distributed under a Creative Commons CC BY license.

Preprints (www.preprints.org) | NOT PEER-REVIEWED | Posted: 20 September 2019 doi:10.20944/preprints201909.0237.v1

1.1 Monitoring of the track-bed

According to the above, a reliable and updated knowledge of the condition of the railway substructure is crucial for a schedule of the maintenance activities that actually addresses the optimization of the productivity while keeping the highest safety standards.

Necessarily, the monitoring procedures that allow for such a knowledge have to comply with cost-benefits considerations. As a result, the quality of the monitoring in terms of dedicated funds is typically related to the rate of utilization of the inspected railway stretch [3]. In such a framework, increasingly efficient inspection techniques are required for lowering the cost-to-benefit ratio, thereby allowing maintainers for a wider assessment of the track-bed conditions over the entire network.

Within this context, visual inspections, even though still widely diffused, represent the traditional monitoring procedure. On-site operators are required to evaluate the condition of various components of the railway track reporting the presence and extent of decay for each structural component. In regard to ballast, this approach allows to judge signs of fragmentation and fouling only at the surface level. However, deep pollution and fragmentation of the aggregates below the surface are neglected.

Nowadays, automatic laser-based systems are employed as an integration to the traditional approach. These systems, mounted onto dedicated diagnostic convoys, permit to record the geometric parameters of the steel rail (i.e., gauge, rail alignment) and, therefore, to observe anomalous deformations along the track. Even though this approach is evidently more robust than performing only visual inspections, it allows a partial and late assessment of the condition of the substructure. Both fouling and fragmentation are in fact detected only at a very advanced stage, i.e. when the deformation of the rails has started.

In view of this, some diagnostic trains are being equipped with additional systems for the direct assessment of the condition of the ballast. Among the other, Ground-Penetrating Radar (GPR) is one of the most acknowledged.

1.1.1 Ground-Penetrating Radar for ballast assessment

GPR is a widespread geophysical technique, which allows to inspect relevant features of the subsurface using information from the propagation of electromagnetic (EM) fields [8]. Characteristics of the specific device and the properties of the tested material, in turn, rule the propagation process. To this extent, the relative dielectric permittivity ε_r and the electric conductivity σ are mainly responsible for the velocity of the propagating EM waves and their attenuation in depth, respectively [9].

Practically, a source inner to the GPR system emits an EM impulse that is partially back-reflected and partially transmitted beyond at any given dielectric contrast encountered throughout the medium. The collection of such diffractive occurrences through a receiving station allows for the imaging of the subsurface features, in both two and three dimensions [8, 9].

First attempts of using GPR as a potential method for assessing the conditions of ballasted railway track-beds date back to first noughties, by literature [10, 11]. In these experimental activities, the surveys have been conducted by using GPR systems with central frequencies below 500 MHz. More recently, high-frequency (1000 MHz to 2000 MHz) air-launched systems have been mostly adopted [12-16], due to relevant advantages observed in terms of results viability and productivity of the surveys.

It is important to observe that the research focus on the subject area has also changed over years [17]. The assessment of the geometry of the track-bed and its overall stability have been firstly investigated

Preprints (www.preprints.org) | NOT PEER-REVIEWED | Posted: 20 September 2019 doi:10.20944/preprints201909.0237.v1

[10, 19], whereas the focus has progressively shifted towards the time-domain [14-16] and frequency-domain [12, 14, 20-24] analysis of the effects of fouling and fragmentation of the track-bed on the signal. In addition to this, new avenues in assessing quality of ballast aggregates have been recently explored by means of simulation-based [25] and numerical models [26].

Although crucial pieces of information were derived from these studies, only few laboratory and test-site activities are reported in literature, to the best of the authors' knowledge. This is most likely due to the high costs and the labor extensiveness of the operations [2, 27, 28].

This work reports the results of an extensive experimental campaign conducted on a test-site located along a real-life railway in Rome, Italy. The main aim of the research is to investigate the viability of GPR in assessing the health conditions of railway track-beds and to evaluate its suitability for implementation into maintenance management programs. In this regard, the effects of fouling and fragmentation of the ballast on the EM signal are analysed and interpreted with particular reference to potential applications in maintenance and monitoring activities. Modelling is finally proposed to estimate fouling content.

Specifically, the specific objectives of this study can be summarised as follows:

- Inferring the influence of fragmentation and fouling of ballasted track-beds on the EM signal as collected by GPR.
- defining the role played by the humidity for the detection of ballast decay;
- providing useful information for the most suitable survey configuration (central frequency of the antenna, polarisation, …) according to the specific survey target.

2. Materials and Methods

The experimental activity was planned and carried out by the Department of Engineering of Roma Tre University, on a railway stretch located within a depot area managed by the Italian National Railways (RFI) S.p.A.

2.1 Inspected material

In order to reproduce different rates of fragmentation, two samples of typical limestone railway ballast were selected for the arrangement of the test site. Specifically, an ex-quarry ballast sample complying with the relevant quality standards from the Italian National Railways [29] and an exhausted ballast that had been removed from service according to the evident deterioration of its aggregates, were used. Fig. 1 shows the grading curves of the samples, achieved following dedicated standards for the sieve method [30], along with the boundaries set by the national standards. The curves GC1 and GC2 define two health conditions standing for a well-graded ballast and a highly fragmented ballast thereby requiring renewal.

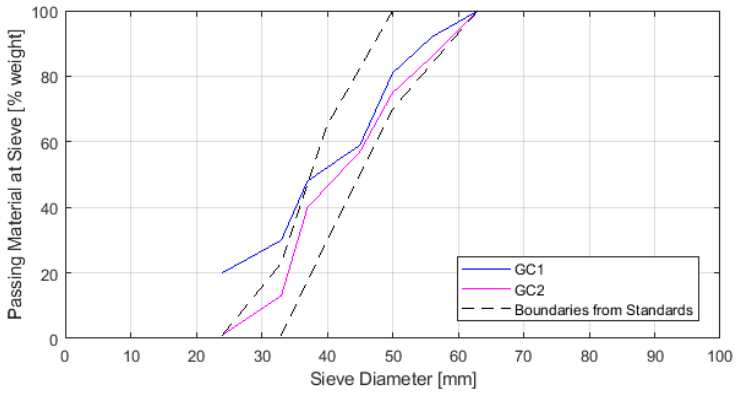

Preprints (www.preprints.org) | NOT PEER-REVIEWED | Posted: 20 September 2019 doi:10.20944/preprints201909.0237.v1

Figure 1. Outcomes of the sieving test on the ballast samples used for the tests.

In addition, different fouling conditions were reproduced using a fine-graded soil, excavated from a depot. It worth noting that the material had been previously removed from inadequate railway subgrades due to the severe uprising of fine particles to the ballast layers. Two fouling conditions representing clean ballast, i.e. all the voids between aggregates are clean from pollution (Fouling Index (FI) = 0%), and fouled ballast, i.e. all the voids are clogged up by the polluting soil (FI=25%), were accounted for testing purposes. The FI is calculated as follows [7]:

$$\mathrm{FI} = P_4 + P_{0.075} \quad (1)$$

where P_4 and $P_{0.075}$ are the percentages in weight of the material passing the 4 mm and the 0.075 mm sieves [22].

2.2 Test site preparation

A 30 m-long section of railway was investigated using GPR. Location and main characteristics of the test-site are shown in Fig. 2. The superstructures is composed of steel rails with a 1.435 m-wide gauge, fastened to mono-block reinforced concrete sleepers spaced 0.60 m each to one another.

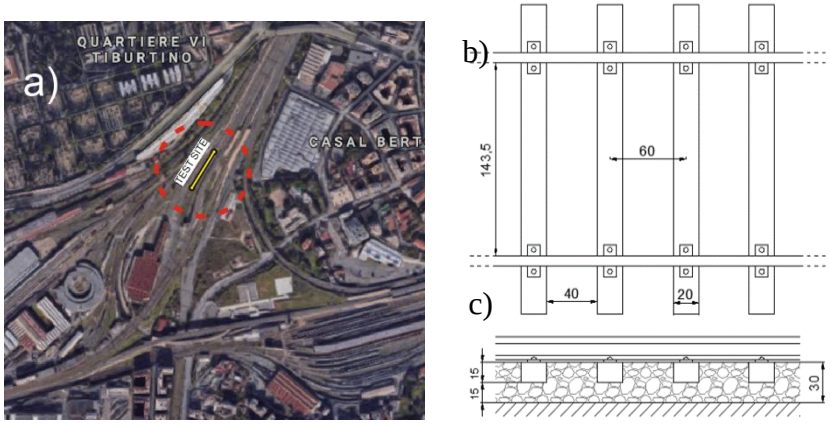

Figure 2. (a) Location of the test-site; (b) plan-view of the inspected railway section; (c) cross-section of the track-bed. The measures are expressed in cm.

The ballast-filled slots comprised between the sleepers in the test-site area were emptied out and re-filled with the test material. This allowed to create 10 different configurations/sub-sections of fouling and fragmentation conditions of the track-bed, each one comprising 3 consecutive slots (Fig. 3).

Preprints (www.preprints.org) | NOT PEER-REVIEWED | Posted: 20 September 2019 doi:10.20944/preprints201909.0237.v1

Figure 3. Preparation of a single sub-section within the test-site area; (a) a set of three slots is emptied out of the original ballast; (b) the slots are filled up again with the test material; (c) the material is arranged and compacted in order to fill all the voids; (d) the re-arranged configuration.

Arrangement of the 10 sub-sections was realised by dividing each volume into two 15 cm-thick layers (see Fig. 2(c)) and varying the physical conditions of each layer.

Moreover, for each of the 10 configurations, three levels of humidity were reproduced, by progressively pouring water onto the test-site. At each round of GPR tests, a sample of material was extracted from a slot, and the moisture was measured in a laboratory environment. In more detail, water contents of 6% (low humidity -LH-), 12% (medium humidity -MH-) and 17% (high humidity -HH-) were reproduced for testing purposes. The main characteristics of each configuration are reported in Tab. 1.

Table 1. Features of the tested configurations

Config.	Layer 1		Layer 2		Humidity
	Grading Curve	*Fouling Index*	*Grading Curve*	*Fouling Index*	
1	GC1	0	GC1	0	LH, MH, HH
2	GC1	0	GC1	0	LH, MH, HH
3	GC1	0	GC1	25	LH, MH, HH
4	GC1	25	GC1	25	LH, MH, HH
5	GC1	0	GC2	0	LH, MH, HH
6	GC2	0	GC2	0	LH, MH, HH
7	GC2	0	GC1	0	LH, MH, HH
8	GC1	0	GC2	0	LH, MH, HH
9	GC2	25	GC2	25	LH, MH, HH
10	GC2	0	GC2	25	LH, MH, HH

GC=grading curve; LH=low humidity; MH=medium humidity; HH=high humidity

More specifically, configurations 1 and 2 were used as a reference of sound ballast, in terms of both fouling and grading. Third and fourth configurations simulated an increasing rate of uprising clogging of the ballast from the subgrade (FI= 0% to 25%). Configurations 5 to 7 reproduced different rates of aggregates fragmentation, i.e. unsuitable deeper layer (e.g. after the process of renewing the top layer), inadequate shallower layer and total fragmentation of the track-bed. Configurations 8 to

Preprints (www.preprints.org) | NOT PEER-REVIEWED | Posted: 20 September 2019 doi:10.20944/preprints201909.0237.v1

10 simulated various conditions of combined decay. The full arrangement of the test-site is shown in Fig. 4.

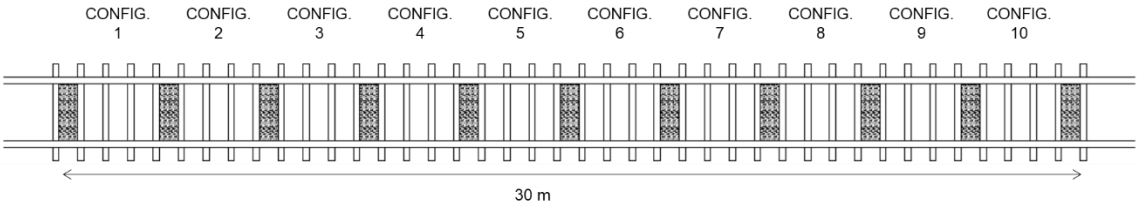

Figure 4. Plan view of the full test-site arrangement.

2.3 Test equipment

The EM response of the various configurations was inspected by towing a pulsed GPR system equipped with high-frequency horn antennas along the test-site. The central frequencies of the antennas were 1000 MHz and 2000 MHz. The system and the antennas were both manufactured by IDS GeoRadar (Part of Hexagon).

The surveys were conducted by means of a hand-towed railway cart (Fig. 5(a)), on which a wooden support permitted to keep the antennas suspended in the air at a fixed height of about 40 cm. The wooden support allowed the rotation of the antenna around the vertical axis. This allowed to reproduce different polarizations of the antenna. To this effect, orientations of 0°, 45° and 90° were created with respect to the towing direction (Fig. 5(b)).

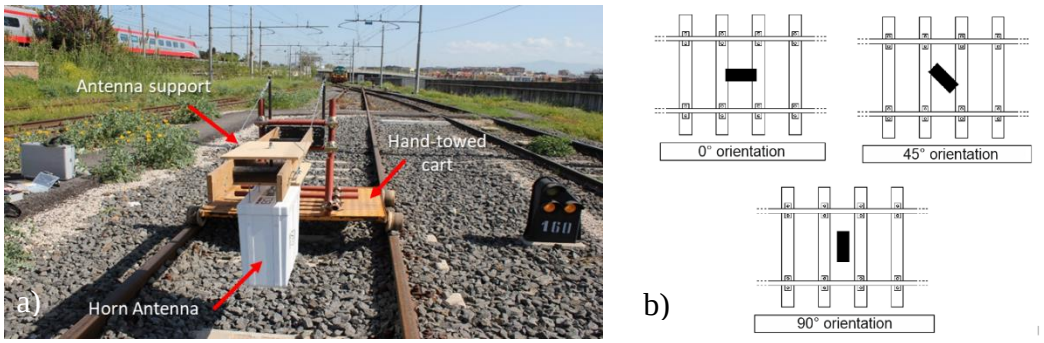

Figure 5. (a) the experimental testing device; (b) tested antenna orientations.

2.4 Survey protocol

Data collection was carried out by towing the GPR system along the full test-site area. Acquisitions were then repeated for each combination of parameter and tested value, as shown in Tab. 2.

Table 2. Parameters and tested values within the data collection process.

Parameter	Tested value
Central frequency	1000 MHz, 2000 MHz
Antenna orientation	0°, 45°, 90°
Humidity	LH, MH, HH

LH=low humidity; MH=medium humidity; HH=high humidity

To this effect, an overall dataset of 18 acquisitions was collected along the 30-m long stretch reported in Fig. 4. The acquisition parameters adopted for the GPR system are reported in Tab. 3, according to the specific frequency.

Preprints (www.preprints.org) | NOT PEER-REVIEWED | Posted: 20 September 2019 doi:10.20944/preprints201909.0237.v1

Table 3. GPR acquisition parameters

Frequency	Parameter	Value
1000 MHz	Time window	25 ns
	Horizontal resolution	0.025 m
	Samples	512
2000 MHz	Time window	15 ns
	Horizontal resolution	0.025 m
	Samples	512

2.5 Data processing

The raw data have been analysed in both time and frequency domains, following the application of a multi-stage processing procedure [31], composed of:

- *Time-zero correction:* for inspections conducted with an air-coupled antenna, direct wave arrival times (time-zero) are not horizontally aligned along the main longitudinal scanning direction, due to the bouncing of the antenna support. This causes a variation of the default height of the antenna along the inspection length. Accordingly, the air layer between the signal source and the surface is removed in order to set a common starting time for each trace.

- *De-wow:* typically, GPR sections show strong lower frequency harmonics ("wow") or initial direct current offsets (Direct Current (DC) shift, DC offset or DC bias), which might cover actual EM reflections. In fact, these harmonics tend to distort the average amplitude of the GPR trace towards values different from zero. De-wow is a stationary low-pass filter that suppresses harmonics with a dominant frequency usually lower than a specific threshold below the Nyquist frequency of the GPR signal.

- *Background removal:* the signal ringing inner to the antenna produces nearly perfect horizontal reflections that might mask actual reflections from real targets and produce unreliable results. Elements surrounding the test-site, such as electricity cables, mobile phones, etc., may generate these horizontal-like reflections. This occurrence is generally referred to as the "background noise". To suppress these artifacts from the signal, the average GPR trace calculated using all the traces in the section is subtracted to every GPR trace, sample by sample.

- *Band-pass filtering:* the signal-to-noise ratio in GPR sections is usually lowered by noise due to the surrounding media and by the inherent loss of the GPR signal, especially at relatively late arrivals. These noise components are generally found to be outside the main working frequency bandwidth of a GPR system. Band-pass filter works by cutting off these side bands from the collected spectrum.

- *Short-time Fourier transform (STFT):* the application of this method allows keeping data information in both time and frequency domain, by tracking the change of frequency spectrum with time (or depth). Such an information is obtained as follows:

$$STFT(t,\omega) = \int_t [x(t) \cdot w(\tau - t)] \cdot e^{-j\omega t} d\tau, \quad (2)$$

Where x is the reflected amplitude, t is the time, ω is the radial frequency, w is the window function and $STFT$ is the frequency energy at time t and frequency ω.

3. Results and discussion

Preprints (www.preprints.org) | NOT PEER-REVIEWED | Posted: 20 September 2019 doi:10.20944/preprints201909.0237.v1

3.1 Influence of the antenna orientation

To isolate the behavior of the track-bed from that related to the concrete sleepers, the only traces collected in the middle of the ballast-filled slots were considered, while those collected on the sleepers or on their proximity were discharged.

Fig. 6 shows the averaged frequency spectra, both for 1000 MHz (in blue) and 2000 MHz (in magenta), with reference to the three orientations of the antenna. As depicted in the figure, the shape of the spectra are found not to be significantly affected by the orientation of the antenna, for both the frequencies. Conversely, the amplitude of the frequency spectrum turned out to be highly affected by this parameter. In regard to the 1000 MHz antenna, the reflected amplitude is observed to increase as the antenna is oriented more transversally with respect to the direction of the rails. On the contrary, a lower reflected intensity is observed for the 2000 MHz antenna in the case of 90° orientation. For this specific orientation, the two antennas returned a response with very similar amplitudes.

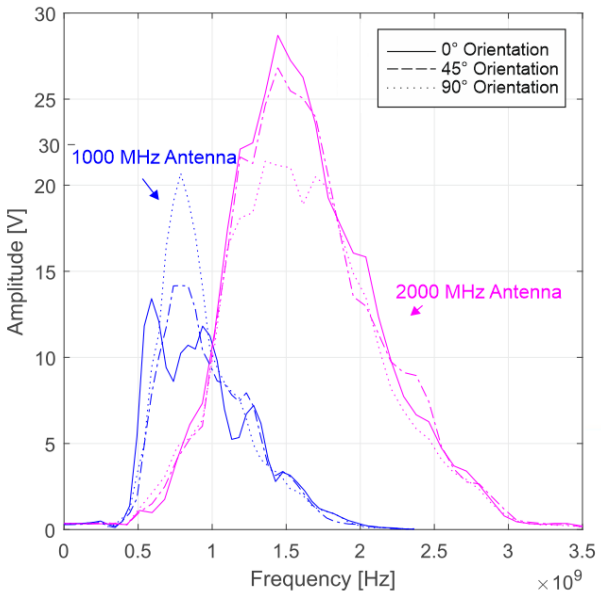

Figure 6. Frequency-domain response collected using the 1000 MHz (blue) and 2000 MHz (magenta) antennas with 0° (solid line), 45° (dashed line) and 90° (dotted line) orientations.

The time-domain influence of the antenna orientation on the EM response of the track-bed is shown in Fig. 7. As a further confirmation of the frequency domain results, the effects from the orientation of the antenna (left to right, in the figure) are much more evident for the 1000 MHz (a-c, first row) as opposed to the 2000 MHz signals (d-f, second row). Indeed, while the latter are not significantly affected by the antenna polarisation, the response from the 1000 MHz inspection returns very different outcomes. In particular, the signal collected using the 0° orientation (a) shows to be seriously affected by the presence of the concrete sleepers that cause clearly distinguishable hyperbolas.

Preprints (www.preprints.org) | NOT PEER-REVIEWED | Posted: 20 September 2019 doi:10.20944/preprints201909.0237.v1

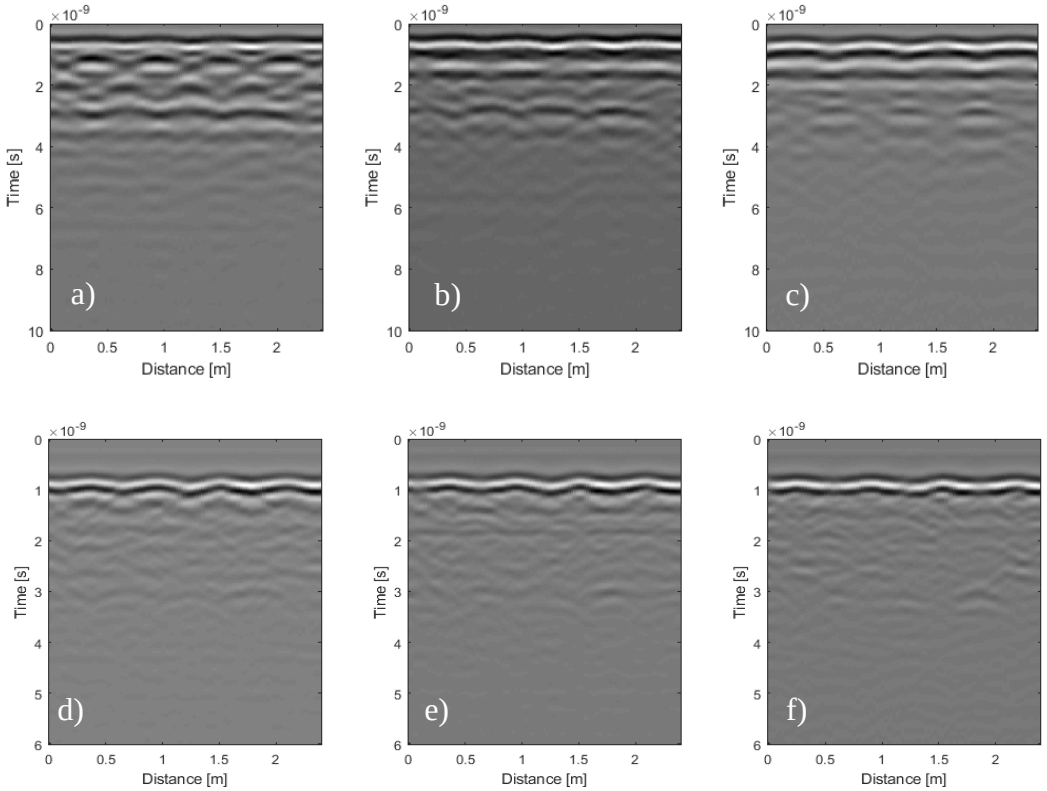

Figure 7. Time-domain response collected over the configuration 1 with 1000 MHz (a-c) and 2000 MHz (d-f) antennas, using 0° (a, d), 45° (b, e) and 90° (c, f) orientations.

On the other hand, transversal polarisation (c) returned a very high reflection from the surface, with only a slight influence from the sleepers. However, the attenuation of the signal in depth turned out to inhibit a clear identification of the bottom of the track-bed. Conversely, 45° (b) orientation turned out to provide the most clear time-domain results, in terms of structural detailing of the track-bed. *Al-Qadi et al.* [33] have given a possible explanation for this occurrence. Indeed, the authors have related this factor to the incidence angle of the EM waves on the rails and the sleepers that, for this orientation, tends to send them away from the antenna.

3.2 Grading-dependent behaviours

As far as the influence of ballast grading is concerned, dry conditions of configurations 1 (GC1) and 6 (GC2) were taken into account to represent sound and crushed ballast, respectively. Moreover, configurations 5 and 7 (1 layer of sound ballast and 1 layer of crushed ballast) were considered in order to reproduce partially-crushed material. Fig. 8 shows the EM response of these configurations in the frequency domain. The frequency spectra reported in the plot have been obtained by averaging the traces collected in the central 15 cm-section of each of the three ballast slots composing the configuration.

Preprints (www.preprints.org) | NOT PEER-REVIEWED | Posted: 20 September 2019 doi:10.20944/preprints201909.0237.v1

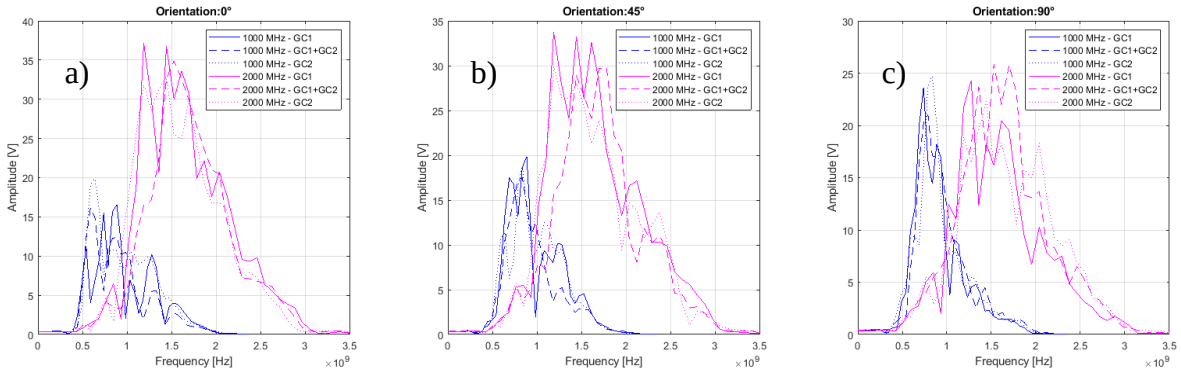

Figure 8. Frequency-domain EM response collected using the 1000 MHz (blue) and 2000 MHz (magenta) antennas with a) 0°, b) 45° and c) 90° orientations, of sound (solid line), averagely-crushed (dashed line) and totally-crushed (dotted line) dry ballast.

Regarding the signal collected by the 1000 MHz antenna (in blue in Fig. 8), the shape of the spectra was found not to vary significantly in relation to the fragmentation rate. This was verified for all the orientations of the antenna.

On the contrary, analysis of the data from the 2000 MHz antenna (in magenta in Fig. 8), allows to identify a dependency between the spectrum shapes and the fragmentation rate. In particular, for all the antenna orientations, the frequency spectra relative to sound ballast (GC1, solid lines in Fig. 8) showed a significant rate of energy at lower frequencies, i.e. in the 1100-1300 MHz frequency range, with respect to the averagely- or totally-crushed configurations (dashed and dotted lines).

Such a grading-dependent behaviour of sound ballast subject to high-frequency EM fields is in agreement with subject-related literature. In fact, this has already been observed in previous research [12, 20, 21] that has related this occurrence with scattering and resonance effects triggered by the specific dimension of the aggregates and air voids. The time-frequency analysis carried out using the STFT approach, as depicted in Fig. 9, demonstrates that for sound ballast (a) most of the energy is focused at a short arrival time (4-6 ns), followed by a gradual attenuation ending up around 14 ns. As the fragmentation of the ballast increases, a quicker attenuation of the signal is observed. In particular, energy drops at 13 ns and 12.5 ns were reported for semi-crushed and totally-crushed configurations (Fig. 9(b,c)).

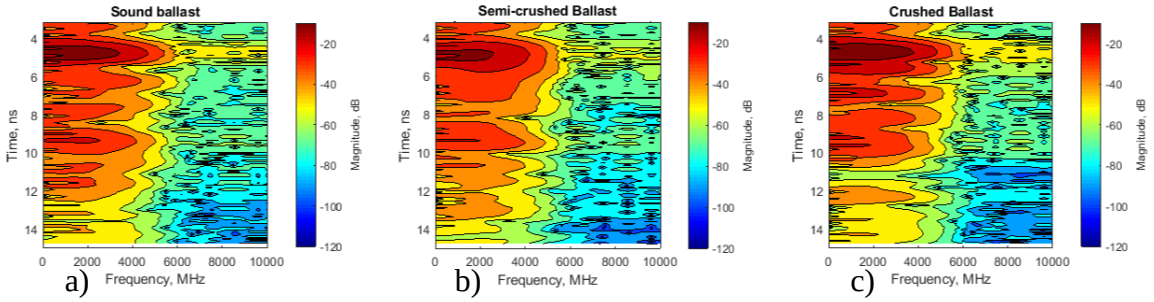

Figure 9. STFT spectra for (a) sound, (b) averagely crushed ballast and (c) totally crushed ballast, collected with 2000 MHz antenna with 45° orientation.

3.3 Fouling/moisture effects

Due to the known physio-chemical attitude of fine-graded materials towards the retention of the humidity [21-23], fouling and moisture are expected to magnify each other's influence on the EM signal. In fact, the more fouled is the track-bed, the less efficient is the drainage of liquids poured

Preprints (www.preprints.org) | NOT PEER-REVIEWED | Posted: 20 September 2019 doi:10.20944/preprints201909.0237.v1

onto the surface but, in turn, the water retained by the polluting material is responsible of severe changes in its dielectric properties. Therefore, the EM effects of the fouling are expected to be significantly more evident in case of high humidity conditions. On the other hand, the effects of water content on the EM response of ballast are expected to be negligible, in absence of pollution.

Following these assumptions, three test configurations at growing fouling conditions have been taken into account at three different rates of humidity. The amplitude of the air-surface reflection was observed along its length for all of these configurations. Results are shown in Fig. 10.

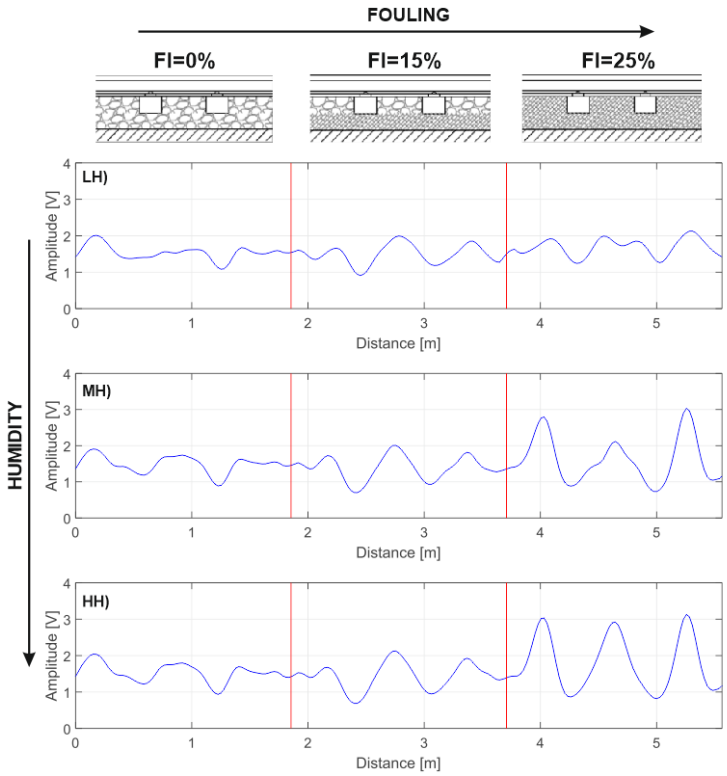

Figure 10. Amplitude of the air-surface reflection for clean (FI=0%), partially-fouled (FI=15%) and totally-fouled (FI=25%) configurations, in low (LH), medium (MH) and high (HH) humidity conditions. Data were collected with a 90° orientation of the 1000 MHz antenna.

The outcomes clearly confirm the initial assumptions, as the influence of the fouling rate (left to right) is much more evident for high humidity (HH) conditions. Similarly, the effects of water content (top to bottom) are most likely to be appreciated in the case of totally-fouled ballast conditions (FI=25%).

In more detail, the variation of the reflection amplitude when the antenna moved from the concrete sleeper to free ballast was taken as a reference for the evaluation of the influence of both fouling and humidity factors [32]. In fact, the behaviour of the amplitude appears as quasi-horizontal for LH, FI=0% conditions, whereas it assumes a sinusoidal shape for HH, FI=25%. In this case, the position of the sleepers is exactly recognizable. To demonstrate this statement quantitatively, the standard deviation of the reflection amplitude is plotted in Fig. 11 against the FI and the moisture.

Preprints (www.preprints.org) | NOT PEER-REVIEWED | Posted: 20 September 2019 doi:10.20944/preprints201909.0237.v1

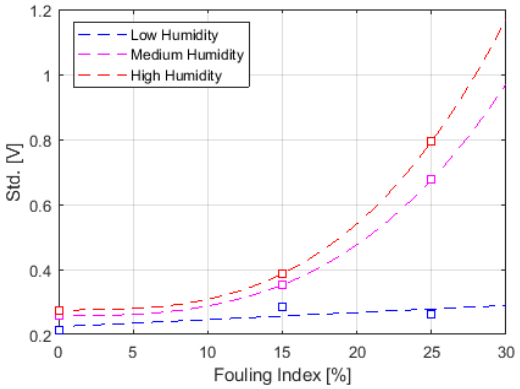

Figure 11. Standard deviation of the surface reflection amplitude against fouling and moisture conditions.

As demonstrated by Fig. 11, standard deviation of the surface reflection variability stands as a viable indicator for predicting the rate of fouling. The polynomial regression reported in Fig. 11 can be analytically expressed as follows:

$$\mathbf{FI} = \sum_{i=0}^{3} \boldsymbol{a_i SD^i}, \tag{3}$$

with FI and SD being the Fouling Index and the Standard Deviation of the surface reflection variability, respectively. The value of the coefficients a_i are reported in Tab. 4.

Table 4 Coefficient a_i in eq. (3).

Humidity	a_3	a_2	a_1	a_0
Low	0.0022	0.2240	0	0
Medium	2.47×10^{-5}	5.24×10^{-5}	0	0.2575
High	3.33×10^{-5}	-4.12×10^{-5}	0	0.2754

The above findings are confirmed by the analysis of the time-frequency data. Fig. 12 shows the application of STFT to GPR traces collected with the 1000 MHz antenna at the centre of the ballast slot at growing rates of fouling (from left to right), in both low (Figs. 12a-c) and high (Figs. 12d-f) humidity conditions. Influence of fouling is found to be not relevant in drier conditions, whereas it turned out to heavily affect the SFTF spectrum of the track-bed under wet conditions. In this specific case, an energy drop is observed already at 10 ns (Fig. 12(f)).

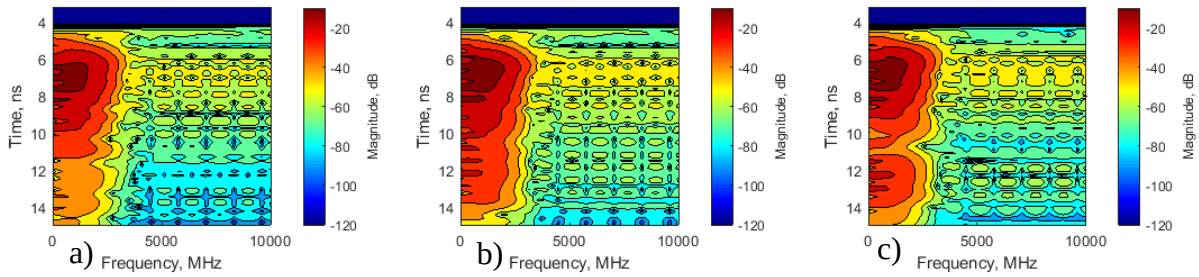

Preprints (www.preprints.org) | NOT PEER-REVIEWED | Posted: 20 September 2019 doi:10.20944/preprints201909.0237.v1

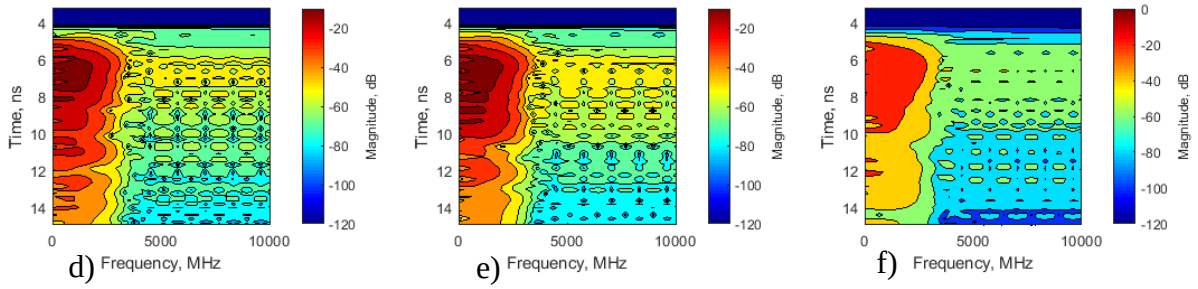

Figure 12. STFT spectra collected with the 1000 MHz antenna at the centre of the ballast slots with FI=0% (a, d), FI=15% (b, e) and FI=25% (c, f), at Low (a-c) and High (d-f) humidity conditions.

4. Conclusions & practical implications

This work reports the experimental activities carried out on a test-site area within a railway depot in Rome, Italy. Specifically, a 30 m-long railway section was divided into 10 sub-sections reproducing different various physical and structural conditions of the track-bed.

Combinations of different scenarios of fragmentation and fouling of the ballast were reproduced. The set-up was then investigated using different multi-frequency (1000, 2000 MHz) GPR horn antenna systems. These were towed along the rail sections by means of a dedicated railway cart that allowed the antenna to be oriented with an angle of 0°, 45° and 90° with respect to the rails.

The effects of the physical conditions of the railway ballast on its EM response is estimated for each scenario using time- and frequency-domain signal processing techniques. Parallel to this, modelling was provided to estimate fouling content.

In regard to the antenna orientation, the influence of the concrete sleepers and the attenuation of the signal in depth for the signal collected with the 1000 MHz antenna, turned out to inhibit a clear identification of the structural details of the track-bed. Amongst all of the orientations, the 45° orientation has provided the most reliable results. On the opposite, it was demonstrated that the high frequency antenna is least affected by its orientation.

Regarding the effects of the aggregate grading on the GPR signal, the shape of the spectra from the 1000 MHz antenna was found not to vary significantly with the fragmentation. Data analysis from the 2000 MHz antenna has proven a dependency of the spectrum shapes on the fragmentation rate. To this effect, the frequency spectra relative to sound ballast were observed to show a greater energy exchange at lower frequencies compared to the averagely- or totally-crushed configurations.

Finally, three test configurations with different fouling conditions have been taken into account at three rates of humidity to assess the influence of these parameters on the EM response of the material investigated. In particular, the variation of the surface reflection amplitude when the antenna moved from the concrete sleeper to free ballast conditions was observed to change with varying conditions of the track-bed. The data analysis permitted to provide an empirical model for the estimation of the FI of the track-bed, based on the spatial standard deviation of the surface reflection amplitude.

Interpretation of the results has shown viability of the GPR method in detecting signs of decay at the network level, thereby proving this technique to be worthy for implementation in asset management systems. Such a conclusion confirms previous research finding on this subject [12-15, 20]. However, this research has pointed out key information in regard to the practical use of an air-coupled GPR system for assessing fragmentation and fouling in railway track-beds.

In this regard, use of high-frequency antenna systems was reported to be promisingly effective in detecting the fragmentation rate of the aggregates. In case of track-beds isolated from the subgrade,

Preprints (www.preprints.org) | NOT PEER-REVIEWED | Posted: 20 September 2019 doi:10.20944/preprints201909.0237.v1

such as the typical modern high-speed tracks, the spectral analysis of the 2000 MHz signal is expected to provide viable information about this particular type of decay.

On the other hand, time-domain and combined time-frequency analyses of the 1000 MHz antenna system, allowed to achieve a reliable indication of the pollution rate of voids within the aggregates. The influence of fouling on the EM response was observed to be particularly relevant for highly-wet conditions. This could imply that monitoring activities may require to be carried out in relatively-dry conditions of the track-bed in order to maximise the effectiveness of the process.

Author Contributions: conceptualization, A.C. and L.B.C.; methodology, A.C. and F.D.; investigation, F.D.; data curation, L.B.C.; writing—original draft preparation, L.B.C.; writing—review and editing, F.D. and A.C.

Acknowledgments: The authors express their deep gratitude to RFI S.p.a. for granting the accessibility to the test-site and the assistance during the surveys. IDS Georadar S.p.a. is also acknowledged for providing part of the survey equipment. Finally, many thanks to Mr. Spartaco Cera for the valuable help in arranging and conducting the experimental operations.

Conflicts of Interest: The authors declare no conflict of interest.

References

1. Indraratna, B. 1st Ralph Proctor lecture of ISSMGE. Railroad performance with special reference to ballast and substructure characteristics. *Transportation Geotechnics*, **2016**, 7, 74-114.
2. Benedetto, A.; Tosti, F.; Bianchini Ciampoli, L.; Calvi, A.; Brancadoro, M.G.; Alani, M.A. Railway ballast condition assessment using ground-penetrating radar – An experimental, numerical simulation and modelling development. *Construction and Building Materials*, **2016**, 140, 508-520.
3. Artagan, S.S.; Bianchini Ciampoli, L.; D'Amico, F.; Calvi, A.; Tosti, F. Non-destructive Assessment and Health Monitoring of Railway Infrastructures. *Surveys in Geophysics*, **2019**, 1-37.
4. Indraratna, B.; Nimbalkar, S.; Coop, M.; Sloan, S.W. A Constitutive model for coal-fouled ballast capturing the effects of particle degradation. *Computer and Geotechnics*, **2014**, 61, 96-107.
5. Selig, E.T.; Waters, J.M. *Track geotechnology and substructure management*, Thomas Telford ed., London, United Kingdom, 1994.
6. Ebrahimi, A.; Tinjum, J.M.; Edil, T.B. Protocol for testing fouled railway ballast in large-scale cyclic triaxial equipment. Geotechnical Testing Journal, 2012, 35.5, 1-9.
7. Selig, E. T.; Dello Russo, V.; Laine. K. J. Sources and Causes of Ballast Fouling, **1992**, Report No. R-805, Association of American Railroads, Technical Center. Chicago, USA.
8. Jol, H. *Ground penetrating radar theory and applications*. 1st ed.; Elsevier: Amsterdam, The Netherlands.
9. Daniels, D.J. *Ground penetrating radar*. 2nd ed.; The Institution of Electrical Engineers: London, United Kingdom.
10. Clark, M.R.; Gillespie, R.; Kemp, T.; McCann, D.M. Forde, M.C. Electromagnetic properties of railway ballast, *NDT & E Int*, **2001**, 34, 305–311.
11. Hugenschmidt, J. Railway track inspection using GPR. *J Appl Geophys*, **2000,** 43(2–4), 147–55.
12. Al-Qadi, I.L.; Xie, W.; Roberts, R. Time-frequency approach for ground penetrating radar data analysis to assess railroad ballast condition. *Research in Nondestructive Evaluation*, **2008**, 19, 219-237.
13. Benedetto, F., Tosti, F., Alani, A.M. An entropy-based analysis of GPR data for the assessment of railway ballast conditions, *IEEE Transactions on Geoscience and Remote Sensing*, **2017**, 55 (7), pp. 3900-3908.
14. Al-Qadi, I.L.; Xie, W.; Roberts, R.; Leng, Z. Data analysis techniques for GPR used for assessing railroad ballast in high radio-frequency environment. *Journal of Transportation Engineering*, **2010**, 136(4), 96-105.
15. Sussmann TR, O'Hara KR, Selig ET. Development of material properties for railway application of ground penetrating radar. Proc Soc Photo-Optical Instrum Eng (SPIE) 2002;4758.
16. Shao, W.; Bouzerdoum, A.; Phung, S.L.; Su, L.; Indraratna, B.; Rujikiatkamjorn, C. Automatic classification of ground-penetrating-radar signals for railway-ballast assessment; *Geoscience and Remote Sensing IEEE Transactions on*, **2011**, 49(10), 3961-3972.
17. Fontul, S.; Fortunato, E.; De Chiara, F.; Burrinha, R.; Baldeiras, M. Railways Track Characterization Using Ground Penetrating Radar, *Procedia Engineering*, **2016**, 143, 1193-1200.
18. De Chiara F. Improvement of railway track diagnosis using ground penetrating radar. 2014. PhD Thesis.

Preprints (www.preprints.org) | NOT PEER-REVIEWED | Posted: 20 September 2019 doi:10.20944/preprints201909.0237.v1

19. Olhoeft, G.R.; Selig, E.T. Ground penetrating radar evaluation of railway track substructure conditions, 9th International Conference on Ground Penetrating Radar (GPR 2002), Santa Barbara, California, 2002, April 29 – 2 May.
20. Bianchini Ciampoli, L., Tosti, F., Brancadoro, M.G., D'Amico, F., Alani, A.M., Benedetto, A. A spectral analysis of ground-penetrating radar data for the assessment of the railway ballast geometric properties, *NDT & E Int*, **2017**, 90, 39-47.
Tosti, F., Benedetto, A., Bianchini Ciampoli, L., Lambot, S., Patriarca, C., Slob, E.C. GPR analysis of clayey soil behaviour in unsaturated conditions for pavement engineering and geoscience applications. *Near Surface Geophysics*, **2016**, 14 (2), pp. 127-144.
21. Patriarca, C., Tosti, F., Velds, C., Benedetto, A., Lambot, S., Slob, E. Frequency dependent electric properties of homogeneous multi-phase lossy media in the ground-penetrating radar frequency range. *Journal of Applied Geophysics*, **2013,** 97, pp. 81-88.
22. Benedetto, A., Tosti, F., Ortuani, B., Giudici, M., Mele, M. Soil moisture mapping using GPR for pavement applications (2013) IWAGPR 2013 - Proceedings of the 2013 7th International Workshop on Advanced Ground Penetrating Radar, art. no. 6601550.
23. Tosti, F; Bianchini Ciampoli, L.; Calvi, A.; Alani, A.M.; Benedetto, A. An investigation into the railway ballast dielectric properties using different GPR antennas and frequency systems, *NDT & E Int*, **2018**, 93, 131-140.
24. Brancadoro, M.G., Bianchini Ciampoli, L., Ferrante, C., Benedetto, A., Tosti, F., Alani, A.M. An Investigation into the railway ballast grading using GPR and image analysis (2017) 9th International Workshop on Advanced Ground Penetrating Radar, IWAGPR 2017 - Proceedings, art. no. 7996043.
25. Benedetto, A., Bianchini Ciampoli, L., Brancadoro, M.G., Alani, A.M., Tosti, F. A Computer-Aided Model for the Simulation of Railway Ballast by Random Sequential Adsorption Process, *Computer-Aided Civil and Infrastructure Engineering*, **2018**, 33 (3), pp. 243-257.
26. Shangguan, P., Al-Qadi, I.L., Leng, Z. Ground-penetrating radar data to develop wavelet technique for quantifying railroad ballast-fouling conditions. *Transportation Research Record* 2289, **2012**, 95-102.
27. Fontul, S.; Fortunato, E.; De Chiara, F. Evaluation of ballast fouling using GPR, 15th International Conference on Ground Penetrating Radar (GPR 2014), Brussels, Belgium, 2014, June 30 – July 4.
28. RFI DTC SICS SP IFS 001A. "Capitolato generale tecnico di appalto delle opere civili" - Sezione 17: Pietrisco per massicciate ferroviarie, 2016.
29. EN 933-1:2012. Tests for geometrical properties of aggregates - Part 1: Determination of particle size distribution - Sieving method. European Committee for Standardization, 2012.
30. Bianchini Ciampoli, L.; Tosti, F.; Economou, N.; Benedetto, F. Signal Processing of GPR Data for Road Surveys. *Geosciences*, **2019**, 96(9), 1-20.
31. Benedetto, A., Tosti, F., Schettini, G., Twizere, C. Evaluation of geotechnical stability of road using GPR (2011) 2011 6th International Workshop on Advanced Ground Penetrating Radar, IWAGPR 2011, art. no. 5963858.
32. Al-Qadi, I.A.; Xie, W.; Roberts, R. Optimization of antenna configuration in multiple-frequency ground penetrating radar system for railroad substructure assessment. *NDT & E Int*, **2010**, 43(1), 20-28.